Local Chern marker for periodic systems

Nicolas Baù ◉ and Antimo Marrazzo ◉*

Dipartimento di Fisica, Università di Trieste, Strada Costiera 11, I-34151 Trieste, Italy

Topological invariants are global properties of the ground-state wave function, typically defined as winding numbers in reciprocal space. Over the years, a number of topological markers in real space have been introduced, allowing to map topological order in heterogeneous crystalline and disordered systems. Notably, even if these formulations can be expressed in terms of lattice-periodic quantities, they can actually be deployed in open boundary conditions only, as in practice they require computing the position operator $\mathbf{r}$ in a form that is ill defined in periodic boundary conditions. Here, we derive a local Chern marker for infinite two-dimensional systems with periodic boundary conditions in the large supercell limit, where the electronic structure is sampled with one single point in reciprocal space. We validate our approach with tight-binding numerical simulations on the Haldane model, including trivial/topological superlattices made of pristine and disordered Chern insulators. The strategy introduced here is very general and could be applied to other topological invariants and quantum-geometrical quantities in any dimension.

I. INTRODUCTION

Topological order is defined by the existence of integer topological invariants that globally characterize the system and cannot be changed under adiabatic transformations. For condensed-matter systems, and electronic structure in particular, topological invariants are often introduced as reciprocal-space integrals of quantum-geometrical quantities that become quantized over closed surfaces. The archetypal topological invariant is the Chern number in two dimensions, which can be written as the integral of the Berry curvature over the Brillouin zone (BZ) torus and it is a $\mathbb{Z}$ integer [1,2]. Even for correlated systems, integer invariants can be obtained by integrating over the boundary conditions, as for the many-body Chern number [3]. Hence, topological invariants are conventionally introduced as global quantities of the system, where the latter is implicitly assumed to be homogeneous. A number of strategies have been proposed to calculate topological invariants in nonhomogeneous or disordered systems [4], such as the switch-function formalism [5–7], methods based on the scattering matrix [8,9] or on the noncommutative index theorem [10–12], the Bott index [13–15], real-space formulas [16,17], and local markers [18].

Notably, nontrivial topology has its most dramatic manifestation in the simplest, and most relevant, nonhomogeneous setting: the interface between a topological phase and a trivial phase, such as vacuum or a trivial semiconductor. For the sake of concreteness, let us consider a quantum anomalous Hall (also known as Chern) insulator in the absence of strong electronic correlations, which is defined by a nonvanishing Chern number, and we place it in contact with a vacuum or with a trivial insulator. As topological invariants cannot change under deformations of the Hamiltonian that do not close the band gap, metallic chiral edge states will appear at the one-dimensional edge separating the trivial from the topological regions. This setting cannot be described at once by any global topological invariant, as the system is clearly made of two, topologically distinct, regions. On the other hand, the locality (or "nearsightedness" according to Kohn [19]) of the ground-state electronic structure hints that it must be possible to probe nontrivial topology, which is also a ground-state property, locally in real space and by using only knowledge from the neighborhood around the region of interest.

Indeed, it has been shown by Bianco and Resta [18] that the Chern number C can be mapped to real space by deriving a topological marker $\mathfrak{C}(\mathbf{r})$. Notably, this is possible not only for topological—i.e., quantized—properties of the electronic structure, but also for the broader set of quantum-geometrical quantities, where a corresponding local real-space marker exists for both insulators and metals. Examples include the geometrical intrinsic part of the anomalous Hall conductivity [20,21], the orbital magnetization [22–25], and the localization tensor [26] which is deeply connected to the quantum metric [27]. Local topological markers can be related to local circular dichroism, which can be experimentally measured [28–30]. The strategy behind the Bianco-Resta marker relies on rewriting the Berry curvature in terms of the operator $\mathcal{P}\mathbf{r}\mathcal{Q}$, where $\mathcal{P}$ and $\mathcal{Q}$ are the projector operators over the occupied and empty orbitals, respectively. Several equivalent formulations of the local Chern marker (LCM) are possible. Here, we report the one developed in Ref. [20],

$$\mathfrak{C}(\mathbf{r}) = -4\pi \, \mathrm{Im} \, \langle \mathbf{r} | \mathcal{P}x\mathcal{Q}y | \mathbf{r} \rangle \quad (1)$$

$$= 4\pi \, \mathrm{Im} \, \langle \mathbf{r} | \mathcal{P}[x, \mathcal{P}][y, \mathcal{P}] | \mathbf{r} \rangle , \quad (2)$$

where x and y are the Cartesian components of the position operator $\mathbf{r}$; the second line is reformulated to emphasize that only occupied states are needed, hence being more suited to numerical implementations. The local Chern number can then

be obtained by calculating the macroscopic average of $\mathfrak{C}(\mathbf{r})$, essentially taking the trace per unit of area Tr_A in a neighborhood around the region of interest. A key aspect of this approach is that the Chern number can be expressed as a *trace*, which can be evaluated locally in real space. At variance with $\mathbf{r}$, the operators $\mathcal{P}\mathbf{r}\mathcal{Q}$ and $[\mathbf{r}, \mathcal{P}]$ are well defined and regular even in periodic boundary conditions (PBCs) [18]. However, in practice, such operators are not directly accessible and are typically constructed by calculating first the position operator $\mathbf{r}$ in a proper basis: Only after, $\mathbf{r}$ is multiplied with the projection operators to obtain Eqs. (1) or (2). Hence, the usual LCM can only be applied to open boundary conditions (OBCs), i.e., for finite samples.

In this paper, we derive an LCM for extended systems in PBCs. Our approach allows calculating space-resolved Chern numbers from large-cell electronic structure simulations, where the BZ is typically sampled with a single point, usually the BZ center Γ. We validate the approach on homogeneous samples and trivial/topological superlattices based on the Haldane model [31], where we examine both pristine and disordered Chern insulating phases. In passing, we provide a simple physical picture that connects the single-point Chern number [32,33] with the Bott index [13–15], and demonstrate that both methods measure the topological obstruction to choose a periodic smooth gauge all over the BZ in the large-cell (i.e., single k-point) limit.

II. LOCAL CHERN MARKER IN PERIODIC BOUNDARY CONDITIONS

A. Single-point local marker

PBCs are often the method of choice for electronic structure calculations. Not only are they the most natural option to study perfect crystals, but they also reduce finite-size effects for noncrystalline systems, such as materials with defects, surfaces, heterojunctions (e.g., in lead-conductor-lead geometries), or amorphous materials. In the case of noncrystalline structures, large periodic cells are used and results are typically checked for convergence with respect to the size of the simulation cell. If the size is large enough, the sampling of the BZ can be reduced to a single point in reciprocal space, typically the Γ point. In this limit, the Chern number can be calculated through single-point formulas as discussed in Ref. [32], We report here the result derived therein,

$$C = -\frac{1}{\pi} \mathrm{Im} \sum_{n=1}^{N_{\mathrm{occ}}} \langle \tilde{u}_{n\mathbf{b}_1} | \tilde{u}_{n\mathbf{b}_2} \rangle, \tag{3}$$

where $\mathbf{b}_{1,2}$ are the reciprocal lattice vectors, $|\tilde{u}_{n\mathbf{b}_j}\rangle$ are the "dual" states of the Hamiltonian eigenstates $|u_{n\Gamma}\rangle$, and represent, in the limit of a large supercell, the states obtained by parallel transport. The sum runs over N_{occ} occupied dual states defined as

$$|\tilde{u}_{n\mathbf{b}_j}\rangle = \sum_{m=1}^{N_{\mathrm{occ}}} S_{mn}^{-1}(\mathbf{b}_j) e^{-i\mathbf{b}_j \cdot \mathbf{r}} |u_{m\Gamma}\rangle, \tag{4}$$

where we introduce the overlap matrix $S_{nm}(\mathbf{b}_j) = \langle u_{n\Gamma}|e^{-i\mathbf{b}_j \cdot \mathbf{r}}|u_{m\Gamma}\rangle$. The dual states enjoy the property $\langle \tilde{u}_{n\mathbf{b}_j}|u_{m\Gamma}\rangle = \delta_{nm}$ and allow fixing a continuous gauge,

essentially adopting a discretized version of the covariant derivative [34,35].

Now we rewrite Eq. (3) as a trace

$$C = -\frac{1}{\pi} \mathrm{Im} \, \mathrm{Tr} \left\{ \sum_{n=1}^{N_{\mathrm{occ}}} |\tilde{u}_{n\mathbf{b}_2}\rangle \langle \tilde{u}_{n\mathbf{b}_1}| \right\}, \tag{5}$$

and we define

$$\tilde{P}_{\mathbf{b}_2,\mathbf{b}_1} = \sum_{n=1}^{N_{\mathrm{occ}}} |\tilde{u}_{n\mathbf{b}_2}\rangle \langle \tilde{u}_{n\mathbf{b}_1}|. \tag{6}$$

In general, $\tilde{P}_{\mathbf{b}_2,\mathbf{b}_1}$ is not a projector but can be written in terms of the projectors $\mathcal{P}_{\mathbf{b}_j} = \sum_{n=1}^{N_{\mathrm{occ}}} |\tilde{u}_{n\mathbf{b}_j}\rangle \langle \tilde{u}_{n\mathbf{b}_j}|$,

$$\tilde{P}_{\mathbf{b}_2,\mathbf{b}_1} = \mathcal{P}_{\mathbf{b}_2} \mathcal{P}_\Gamma \mathcal{P}_{\mathbf{b}_1}, \tag{7}$$

where $\mathcal{P}_\Gamma = \sum_{n=1}^{N_{\mathrm{occ}}} |u_{n\Gamma}\rangle \langle u_{n\Gamma}|$. We exploit the cyclic property of the trace and write the single-point Chern number as

$$C = -\frac{1}{2\pi} \mathrm{Im} \, \mathrm{Tr} \{ [\mathcal{P}_{\mathbf{b}_1}, \mathcal{P}_{\mathbf{b}_2}] \mathcal{P}_\Gamma \}. \tag{8}$$

Finally, the LCM can be evaluated by taking the macroscopic average (i.e., the local trace per unit of area) of

$$\mathcal{C}(\mathbf{r}) = -\frac{1}{2\pi} \mathrm{Im} \, \langle \mathbf{r}|[\mathcal{P}_{\mathbf{b}_1}, \mathcal{P}_{\mathbf{b}_2}] \mathcal{P}_\Gamma |\mathbf{r}\rangle. \tag{9}$$

Equation (9) is manifestly gauge invariant and perspicuous: A nonvanishing local Chern number arises when $\mathcal{P}_{\mathbf{b}_1}$ and $\mathcal{P}_{\mathbf{b}_2}$ *locally* do not commute. In fact, only in the trivial phase is it possible to choose a periodic smooth gauge such that $\mathcal{P}_{\mathbf{b}_1} = \mathcal{P}_{\mathbf{b}_2}$.

B. Relation with the Bott index

Notably, this brings some insights on the common approach of calculating the Chern number of noncrystalline systems through the Bott index [15,36–40], which measures the commutativity of projected position operators $U = \mathcal{P}_\Gamma e^{\frac{i2\pi}{L} x} \mathcal{P}_\Gamma$ and $V = \mathcal{P}_\Gamma e^{\frac{i2\pi}{L} y} \mathcal{P}_\Gamma$. Indeed, if we take the $\mathcal{P}_{\mathbf{b}_1}$ and $\mathcal{P}_{\mathbf{b}_2}$ operators as defined above Eq. (7) but adopt a periodic gauge, we obtain the U and V operators appearing in the Bott index, as by definition of the direct and reciprocal lattice vectors $\mathbf{a}_i \cdot \mathbf{b}_j = 2\pi \delta_{ij}$. While Toniolo has mathematically demonstrated the formal equivalence between the Bott index and the Chern number [40,41], Eqs. (8) and (9) provide a more physical explanation for why the noncommutativity of the projected position operators is related to the Chern number of noncrystalline systems: These U and V operators are essentially the ground-state projector transported from the BZ center to the BZ boundary with the periodic gauge. As said above for the $\mathcal{P}_{\mathbf{b}_1}, \mathcal{P}_{\mathbf{b}_2}$ operators, in the presence of nonvanishing Chern numbers the gauge cannot be chosen to be simultaneously periodic and smooth over all the BZ, hence the two operators cannot commute. Hence, the single-point Chern number and the Bott index ultimately measure the same phenomenon: the topological obstruction to choose a periodic smooth gauge all over the BZ in the limit where the BZ shrinks to a single point.

In addition, Ref. [39] reports that performing singular value decomposition (SVD) on the projected position operators improves the numerical stability of the Bott index calculation

and is hence adopted in their study; no theoretical justification was provided therein, but from the point of view of Eq. (8) that can be understood as a way to invert the overlap matrix appearing in Eq. (4) and perform a single-point covariant derivative. However, we emphasize that the formula for the Bott index [see Eq. (4) of Ref. [39]] still differs substantially from our PBC LCM introduced in Eq. (9), including the fact that the Bott index calculates a logarithm and does not lead to a space-resolved local marker.

C. Finite-sample limit

We now consider the limit of an infinitely large supercell in PBC where a finite sample is surrounded by vacuum, so $x, y \ll L$ whenever the wave function is not zero and the sample is centered in the middle of a square cell. We can expand the projectors up to order L^{-2} in the supercell size

$$\mathcal{P}_{\mathbf{b}_j} \approx \mathcal{P}_\Gamma + \frac{2\pi i}{L}[\mathcal{P}_\Gamma, r_j] - \frac{2\pi^2}{L^2}[r_j, [r_j, \mathcal{P}_\Gamma]], \quad (10)$$

and use the expression in Eq. (9). Our PBC Chern marker essentially converges to the Bianco-Resta OBC Chern marker of Eq. (2) (for the full calculation, see the Supplemental Material [42]):

$$\mathcal{C}(\mathbf{r}) \underset{x,y \ll L}{=} -4\pi \, \text{Im} \, \langle \mathbf{r}| \, \mathcal{P}_\Gamma x(\mathbb{I} - \mathcal{P}_\Gamma) y \, |\mathbf{r}\rangle + \mathcal{O}(L^{-3}). \quad (11)$$

D. Symmetric formula

Before discussing numerical results, we introduce a "symmetric" version of our PBC marker, where we start from the corresponding "symmetric" single-point Chern number

$$C^{(\text{sym})} = \frac{-1}{4\pi} \text{Im} \sum_{n=1}^{N_{\text{occ}}} (\langle \tilde{u}_{n\mathbf{b}_1}| - \langle \tilde{u}_{n-\mathbf{b}_1}|)(|\tilde{u}_{n\mathbf{b}_2}\rangle - |\tilde{u}_{n-\mathbf{b}_2}\rangle),$$
$$(12)$$

and define the operator

$$\bar{P} = \sum_{\sigma_1 = \pm} \sum_{\sigma_2 = \pm} \sigma_1 \sigma_2 \tilde{P}_{\sigma_2 \mathbf{b}_2, \sigma_1 \mathbf{b}_1}$$
$$= \frac{1}{2} \left(\sum_{\sigma_1 = \pm} \sum_{\sigma_2 = \pm} \sigma_1 \sigma_2 [\mathcal{P}_{\sigma \mathbf{b}_1}, \mathcal{P}_{\sigma_2 \mathbf{b}_2}] \right) \mathcal{P}, \quad (13)$$

where we generalize Eq. (6) as

$$\tilde{P}_{\pm\mathbf{b}_2, \pm\mathbf{b}_1} = \sum_{n=1}^{N_{\text{occ}}} |\tilde{u}_{n\pm\mathbf{b}_2}\rangle \langle \tilde{u}_{n\pm\mathbf{b}_1}|. \quad (14)$$

Here, the term "symmetric" refers to the symmetric derivative (as opposed to the right-hand, i.e., "asymmetric," derivative) used to calculate the Berry curvature when the single-point limit is taken [32]. By performing similar steps as done for Eq. (9), one obtains a symmetric marker:

$$C^{(\text{sym})}(\mathbf{r}) = -\frac{1}{4\pi} \text{Im} \, \langle \mathbf{r}|\bar{P}|\mathbf{r}\rangle$$
$$= -\frac{1}{8\pi} \text{Im} \, \langle \mathbf{r}| \left([\mathcal{P}_{\mathbf{b}_1}, \mathcal{P}_{\mathbf{b}_2}] + [\mathcal{P}_{-\mathbf{b}_1}, \mathcal{P}_{-\mathbf{b}_2}] \right.$$
$$\left. - [\mathcal{P}_{-\mathbf{b}_1}, \mathcal{P}_{\mathbf{b}_2}] - [\mathcal{P}_{\mathbf{b}_1}, \mathcal{P}_{-\mathbf{b}_2}] \right) \mathcal{P}_\Gamma \, |\mathbf{r}\rangle. \quad (15)$$
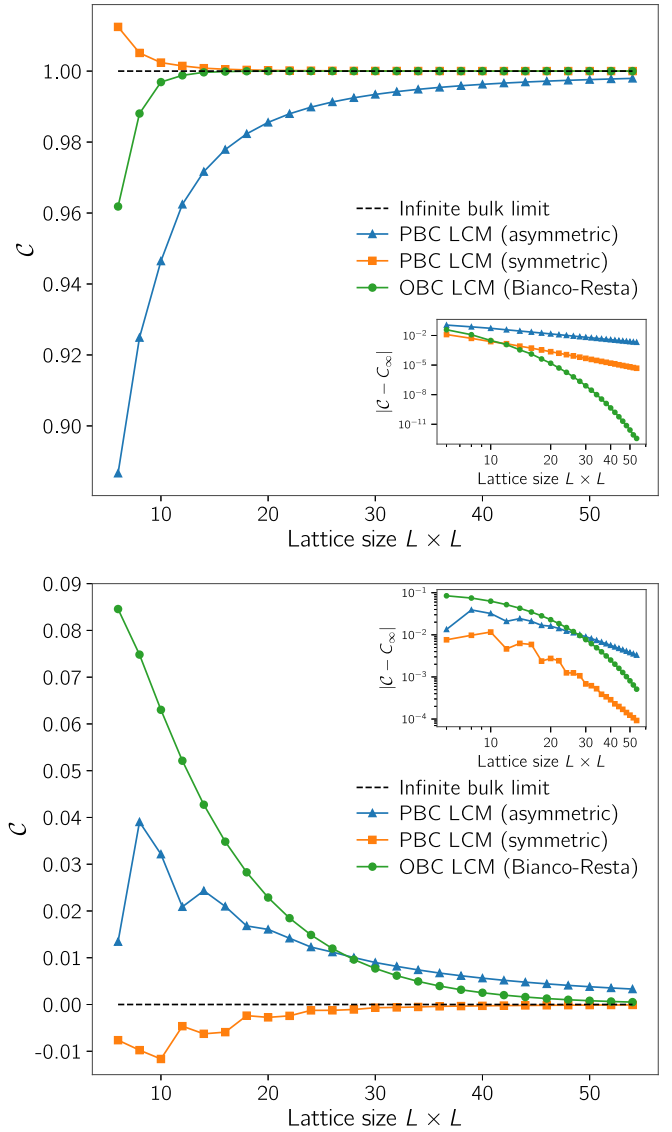

FIG. 1. Convergence of the local Chern marker in periodic boundary conditions for the topological and trivial phase, compared with the Bianco-Resta marker in open boundary conditions. Both the asymmetric and symmetric formulas converge with the supercell linear size L as a power law, where the symmetric version is notably faster.

III. NUMERICAL RESULTS

We validate our approach with tight-binding simulations on the Haldane model [31], which describes electrons hopping on a two-dimensional (2D) honeycomb lattice with a staggered magnetic flux. The parameters of the model are the nearest-neighbor hopping $t = 1$, the on-site energy term $\pm\Delta$ with opposite signs on the two sublattices, and the second-nearest-neighbor hopping term $t_2 e^{i\phi}$ where $t_2 = 0.15$. We release [43] a PYTHON implementation of the LCM PBC in the STRAW-BERRYPY [44] package, which is interfaced with two popular tight-binding software engines such as PYTHTB [45] and TB-MODELS [46,47], and it can be easily interfaced to other codes.

In Fig. 1, we report the convergence of our PBC LCM calculated in a single cell (two sites) in the middle of the bulk, in its symmetric [Eq. (15)] and asymmetric implementation
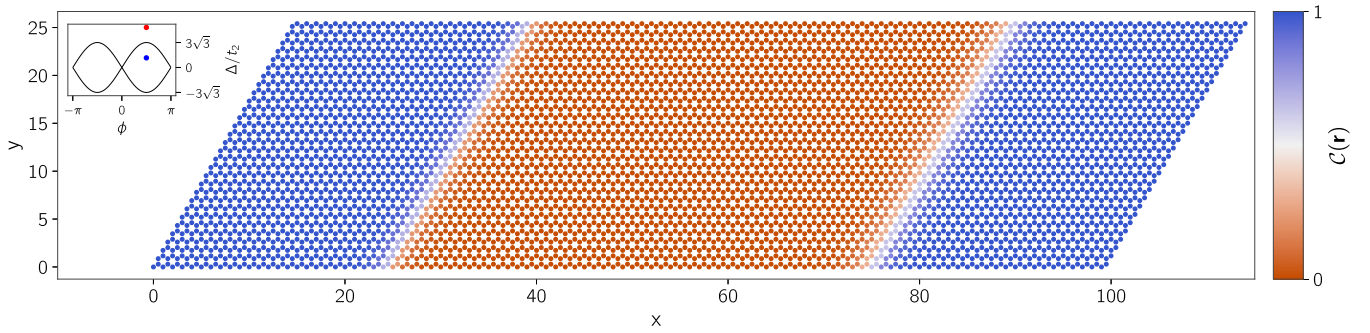
FIG. 2. Local Chern marker for a 6000-site superlattice of the pristine Haldane model made of topological and trivial stripes in periodic boundary conditions. The left and right regions are topological (Chern number $C = 1$) while the center is trivial ($C = 0$); one-dimensional metallic edge states separate the regions with different Chern numbers. The inset displays the model parameters used for the trivial (red) and topological (blue) regions.

[Eq. (9)], with respect to the supercell size. We also compare it with the Bianco-Resta Chern marker [18] calculated on finite samples within OBC corresponding to the same number of sites. The convergence of the PBC LCM is described by a power law: For this choice of the Hamiltonian parameters the power is about -3.6 for the topological and about -2.7 for the trivial phase if evaluated via the symmetric formula [Eq. (15)], while values are about half in the asymmetric version [Eq. (9)]. The value of the power depends on the magnitude of the gap, with larger gaps leading to faster convergence; in general, small lattice sizes are sufficient to infer the topological phase with accuracy. As for the single-point Chern number [32,33], the symmetric formula [Eq. (15)] converges much faster than the asymmetric version [Eq. (9)], hence in the following we always use Eq. (15).

Then we consider the more challenging case of a topological/trivial superlattice, where the system is perfectly periodic along one direction while it is made of alternating topological ($\Delta = 0.3$) and trivial ($\Delta = 1.25$) regions along the other. The results for a 6000-site supercell are reported in Fig. 2. The PBC LCM neatly charts the topological landscape in real space and distinguishes the topological from the trivial region, even close to the boundary of the cell where Eqs. (1) and (2) would dramatically fail. The left and right boundaries of the cell are connected by PBC and the marker is continuous; topologically protected metallic 1D channels are present at about $1/3$ and $2/3$ of the cell along the direction x, precisely where the topological marker changes value. Last, we validate our approach for a nonhomogeneous *and* disordered system. We consider a 5000-site periodic supercell of the Haldane model ($\Delta = 0.2$, $\phi = 0.65\pi$) made of disks of radius $R = 13$ (in units of the lattice parameter) centered on the Bravais lattice with strong ($W = 10$) Anderson disorder [48,49], embedded in a weakly disordered ($W = 1$) matrix. Disorder is introduced through a random on-site term uniformly distributed in $[-W/2, W/2]$. From single-point Chern number calculations we know that extended systems described by those Hamiltonian parameters would be respectively in the topological phase ($C = 1$) for weak disorder and in the trivial phase ($C = 0$) for strong disorder: Hence, we expect our inhomogeneous system to display topologically trivial islands, embedded in a topologically nontrivial matrix. This setting models topological insulators where the concentration

of impurities or defects is not homogeneous (local damage), and locally sufficiently higher to drive the system to the trivial phase. The presence of disorder and metallic interfaces may lead to a gapless density of states over large areas, so we adopt the usual smearing technique similarly to what has been done in Ref. [20] to study the locality of the anomalous Hall conductivity and improve the convergence with respect to the system size. In the presence of smearing, the projectors $\mathcal{P}_{\mathbf{b}_j}$ sum over all the Hamiltonian eigenstates with a Fermi-Dirac occupation function $f(\epsilon_n, T, \mu)$, where ϵ_n is the eigenvalue corresponding to the nth eigenstate, T is a fictitious temperature, and μ is the chemical potential. In addition, we introduce an upper cutoff by discarding the empty states with small occupations [for which $f(\epsilon_n, T, \mu) < f_c$ where we set $f_c = 0.1$], so that the projectors appearing in Eqs. (9) and (15) take the form

$$\mathcal{P}_\Gamma = \sum_{n:f(\epsilon_n,T,\mu)<f_c} f(\epsilon_n, T, \mu) |u_{n\Gamma}\rangle \langle u_{n\Gamma}|, \quad (16)$$

$$\mathcal{P}_{\mathbf{b}_j} = \sum_{n:f(\epsilon_n,T,\mu)<f_c} f(\epsilon_n, T, \mu) |\tilde{u}_{n\mathbf{b}_j}\rangle \langle \tilde{u}_{n\mathbf{b}_j}|. \quad (17)$$

We report in Fig. 3 the numerical results: The PBC LCM is equal to one in the low-disorder regions and vanishing in the strong-disorder circular regions, where Anderson disorder is sufficiently strong to locally destroy the nontrivial topology. As the trivial islands are centered on the Bravais lattice, the PBC marker correctly displays them at the four corners of the supercell (a task that could not be achieved with the Bianco-Resta OBC marker), hence demonstrating that it correctly treats the position operator in PBCs while truly being a local marker.

IV. CONCLUSIONS

In conclusion, we have shown that topological order can be probed locally also in PBCs by means of a simple space-resolved marker, that is capable of charting electronic topology in inhomogeneous and/or disordered systems. Our PBC LCM is based on the ground-state electron distribution only and is derived from the single-point Chern number [32,33], hence being very suited to large-scale *ab initio* electronic structure simulations; that is, it is relevant for the study of amorphous topological materials [4,50,51], quasicrystals
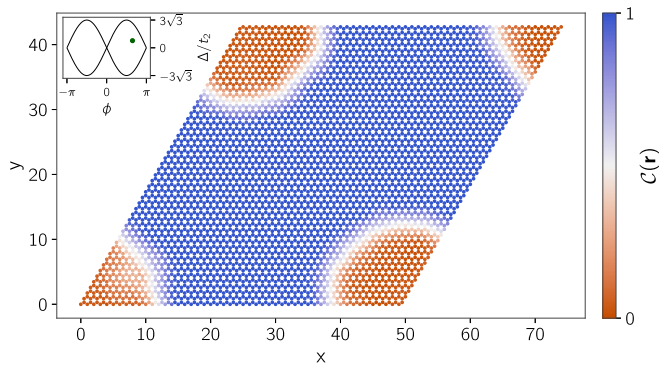
FIG. 3. Local Chern marker for a 5000-site supercell of the Haldane model with Anderson disorder W in periodic boundary conditions. The system is made of disks of radius $R = 13$ in the trivial phase (Chern number $C = 0$) centered on the Bravais lattice, embedded in a topologically nontrivial matrix ($C = 1$); circular metallic edge states separate the two regions with different Chern numbers. The parameters of the Haldane model are constant everywhere ($\Delta = 0.2$, $\phi = 0.65\pi$), while the topological and trivial regions experience respectively weak ($W = 1$) and strong ($W = 10$) Anderson disorder. The smearing temperature is set to $T = 0.05$ and macroscopic averages are performed over a circular region of radius $r = 3$.

[38,39], and in the presence of defects or interfaces. Crucially, our formula contains the operator **r** only as an exponent in $e^{i\mathbf{b}_{1,2}\cdot\mathbf{r}}$, which is known to be the correct approach to treat the position operator in PBCs [52,53] and is related to the modern theory of polarization based on the Berry phase [54]. We note that the PBC position operator has already proved to be key in calculating topological invariants in real space [16], also for interacting systems [55,56]. We have also provided physical insights on the connection between the PBC single-point/local Chern invariants and the Bott index: Measuring the noncommutativity of the projected position operators is essentially measuring the impossibility of choosing a smooth gauge all over the BZ in the limit of a large supercell with single-point sampling. Finally, we emphasize that our approach is potentially very general and could be applied to any geometrical and topological quantity of the electronic structure, in any dimension. The only requirement to develop similar PBC local markers is that the given quantity must be a ground-state bulk property of the system and admit a single-point formula in the large supercell limit.

ACKNOWLEDGMENTS

[1] D. Vanderbilt, *Berry Phases in Electronic Structure Theory: Electric Polarization, Orbital Magnetization and Topological Insulators* (Cambridge University Press, Cambridge, UK, 2018).

[2] B. Bernevig and T. Hughes, *Topological Insulators and Topological Superconductors* (Princeton University Press, Princeton, NJ, 2013).

[3] Q. Niu, D. J. Thouless, and Y.-S. Wu, Quantized Hall conductance as a topological invariant, Phys. Rev. B **31**, 3372 (1985).

[4] P. Corbae, J. D. Hannukainen, Q. Marsal, D. Muńoz-Segovia, and A. G. Grushin, Amorphous topological matter: Theory and experiment, Europhys. Lett. **142**, 16001 (2023).

[5] P. Elbau and G. M. Graf, Equality of bulk and edge Hall conductance revisited, Commun. Math. Phys. **229**, 415 (2002).

[6] C. Tauber, Effective vacua for Floquet topological phases: A numerical perspective on the switch-function formalism, Phys. Rev. B **97**, 195312 (2018).

[7] L. Jezequel, C. Tauber, and P. Delplace, Estimating bulk and edge topological indices in finite open chiral chains, J. Math. Phys. **63**, 121901 (2022).

[8] I. C. Fulga, F. Hassler, and A. R. Akhmerov, Scattering theory of topological insulators and superconductors, Phys. Rev. B **85**, 165409 (2012).

[9] I. C. Fulga, F. Hassler, A. R. Akhmerov, and C. W. J. Beenakker, Scattering formula for the topological quantum number of a disordered multimode wire, Phys. Rev. B **83**, 155429 (2011).

[10] J. E. Avron, R. Seiler, and B. Simon, Charge deficiency, charge transport and comparison of dimensions, Commun. Math. Phys. **159**, 399 (1994).

[11] J. Avron, R. Seiler, and B. Simon, The index of a pair of projections, J. Funct. Anal. **120**, 220 (1994).

[12] H. Katsura and T. Koma, The noncommutative index theorem and the periodic table for disordered topological insulators and superconductors, J. Math. Phys. **59**, 031903 (2018).

[13] M. B. Hastings and T. A. Loring, Almost commuting matrices, localized Wannier functions, and the quantum Hall effect, J. Math. Phys. **51**, 015214 (2010).

[14] M. B. Hastings and T. A. Loring, Topological insulators and C^* algebras: Theory and numerical practice, Ann. Phys. **326**, 1699 (2011).

[15] T. A. Loring and M. B. Hastings, Disordered topological insulators via C^*-algebras, Europhys. Lett. **92**, 67004 (2010).

[16] E. Prodan, T. L. Hughes, and B. A. Bernevig, Entanglement spectrum of a disordered topological Chern insulator, Phys. Rev. Lett. **105**, 115501 (2010).

[17] E. Prodan, Non-commutative tools for topological insulators, New J. Phys. **12**, 065003 (2010).

[18] R. Bianco and R. Resta, Mapping topological order in coordinate space, Phys. Rev. B **84**, 241106(R) (2011).

[19] W. Kohn, Density functional and density matrix method scaling linearly with the number of atoms, Phys. Rev. Lett. **76**, 3168 (1996).

[20] A. Marrazzo and R. Resta, Locality of the anomalous Hall conductivity, Phys. Rev. B **95**, 121114(R) (2017).

[21] T. Rauch, T. Olsen, D. Vanderbilt, and I. Souza, Geometric and nongeometric contributions to the surface anomalous Hall conductivity, Phys. Rev. B **98**, 115108 (2018).

[22] R. Bianco and R. Resta, Orbital magnetization as a local property, Phys. Rev. Lett. **110**, 087202 (2013).

[23] A. Marrazzo and R. Resta, Irrelevance of the boundary on the magnetization of metals, Phys. Rev. Lett. **116**, 137201 (2016).

[24] R. Bianco and R. Resta, Orbital magnetization in insulators: Bulk versus surface, Phys. Rev. B **93**, 174417 (2016).

[25] D. Seleznev and D. Vanderbilt, Towards a theory of surface orbital magnetization, Phys. Rev. B **107**, 115102 (2023).

[26] A. Marrazzo and R. Resta, Local theory of the insulating state, Phys. Rev. Lett. **122**, 166602 (2019).

[27] J. P. Provost and G. Vallee, Riemannian structure on manifolds of quantum states, Commun. Math. Phys. **76**, 289 (1980).

[28] O. Pozo, C. Repellin, and A. G. Grushin, Quantization in chiral higher order topological insulators: Circular dichroism and local Chern marker, Phys. Rev. Lett. **123**, 247401 (2019).

[29] Q. Marsal, D. Varjas, and A. G. Grushin, Topological Weaire-Thorpe models of amorphous matter, Proc. Natl. Acad. Sci. USA **117**, 30260 (2020).

[30] P. Molignini, B. Lapierre, R. Chitra, and W. Chen, Probing Chern number by opacity and topological phase transition by a nonlocal Chern marker, SciPost Phys. Core **6**, 059 (2023).

[31] F. D. M. Haldane, Model for a quantum Hall effect without Landau levels: Condensed-matter realization of the "parity anomaly", Phys. Rev. Lett. **61**, 2015 (1988).

[32] D. Ceresoli and R. Resta, Orbital magnetization and Chern number in a supercell framework: Single **k**-point formula, Phys. Rev. B **76**, 012405 (2007).

[33] R. Favata and A. Marrazzo, Single-point spin Chern number in a supercell framework, Electron. Struct. **5**, 014005 (2023).

[34] N. Sai, K. M. Rabe, and D. Vanderbilt, Theory of structural response to macroscopic electric fields in ferroelectric systems, Phys. Rev. B **66**, 104108 (2002).

[35] I. Souza, J. Íñiguez, and D. Vanderbilt, Dynamics of Berry-phase polarization in time-dependent electric fields, Phys. Rev. B **69**, 085106 (2004).

[36] R. Exel and T. A. Loring, Invariants of almost commuting unitaries, J. Funct. Anal. **95**, 364 (1991).

[37] J. Bellissard, A. van Elst, and H. Schulz-Baldes, The noncommutative geometry of the quantum Hall effect, J. Math. Phys. **35**, 5373 (1994).

[38] H. Huang and F. Liu, Quantum spin Hall effect and spin Bott index in a quasicrystal lattice, Phys. Rev. Lett. **121**, 126401 (2018).

[39] H. Huang and F. Liu, Theory of spin Bott index for quantum spin Hall states in nonperiodic systems, Phys. Rev. B **98**, 125130 (2018).

[40] D. Toniolo, On the Bott index of unitary matrices on a finite torus, Lett. Math. Phys. **112**, 126 (2022).

[41] D. Toniolo, Time-dependent topological systems: A study of the Bott index, Phys. Rev. B **98**, 235425 (2018).

[42] See Supplemental Material at http://link.aps.org/supplemental/10.1103/PhysRevB.109.014206 for details of the expansion of the LCM in the limit of a finite system in a large periodic supercell with vacuum, which includes Refs. [18,57].

[43] The calculation of the local Chern marker in periodic boundary conditions is available in version 0.3.0 of the STRAWBERRYPY code package https://github.com/strawberrypy-developers/strawberrypy/releases/tag/v0.3.0.

[44] The STRAWBERRYPY code package is available at https://github.com/strawberrypy-developers/strawberrypy.git.

[45] The PYTHTB code package is available at http://www.physics.rutgers.edu/pythtb/about.html.

[46] D. Gresch, Q. S. Wu, G. W. Winkler, R. Häuselmann, M. Troyer, and A. A. Soluyanov, Automated construction of symmetrized Wannier-like tight-binding models from *ab initio* calculations, Phys. Rev. Mater. **2**, 103805 (2018).

[47] The TBMODELS code package is available at https://tbmodels.greschd.ch/en/latest/index.html.

[48] E. Abrahams, P. W. Anderson, D. C. Licciardello, and T. V. Ramakrishnan, Scaling theory of localization: Absence of quantum diffusion in two dimensions, Phys. Rev. Lett. **42**, 673 (1979).

[49] B. Hetényi, S. Parlak, and M. Yahyavi, Scaling and renormalization in the modern theory of polarization: Application to disordered systems, Phys. Rev. B **104**, 214207 (2021).

[50] P. Corbae, S. Ciocys, D. Varjas, E. Kennedy, S. Zeltmann, M. Molina-Ruiz, S. M. Griffin, C. Jozwiak, Z. Chen, L.-W. Wang, A. M. Minor, M. Scott, A. G. Grushin, A. Lanzara, and F. Hellman, Observation of spin-momentum locked surface states in amorphous Bi_2Se_3, Nat. Mater. **22**, 200 (2023).

[51] M. Costa, G. R. Schleder, M. Buongiorno Nardelli, C. Lewenkopf, and A. Fazzio, Toward realistic amorphous topological insulators, Nano Lett. **19**, 8941 (2019).

[52] R. Resta, Quantum-mechanical position operator in extended systems, Phys. Rev. Lett. **80**, 1800 (1998).

[53] A. A. Aligia and G. Ortiz, Quantum mechanical position operator and localization in extended systems, Phys. Rev. Lett. **82**, 2560 (1999).

[54] R. Resta, Macroscopic polarization in crystalline dielectrics: The geometric phase approach, Rev. Mod. Phys. **66**, 899 (1994).

[55] A. A. Aligia, Topological invariants based on generalized position operators and application to the interacting Rice-Mele model, Phys. Rev. B **107**, 075153 (2023).

[56] I. Gilardoni, F. Becca, A. Marrazzo, and A. Parola, Real-space many-body marker for correlated $\mathbb{Z}_2$ topological insulators, Phys. Rev. B **106**, L161106 (2022).

[57] A. L. Fetter and J. D. Walecka, *Quantum Theory of Many-Particle Systems* (McGraw-Hill, Boston, 1971).